Characterizing CDK12-Mutated Prostate Cancers

Pasquale Rescigno[1,2], Bora Gurel[1], Rita Pereira[1], Mateus Crespo[1], Jan Rekowski[1], Mattia Rediti[1], Maialen Barrero[1], Joaquin Mateo[3], Diletta Bianchini[2], Carlo Messina[1], Maria D. Fenor de la Maza[1,2], Khobe Chandran[2], Juliet Carmichael[1,2], Christina Guo[1,2], Alec Paschalis[1,2], Adam Sharp[1,2], George Seed[1], Ines Figueiredo[1], Maryou Lambros[1,2], Susana Miranda[1,2], Ana Ferreira[1], Claudia Bertan[1], Ruth Riisnaes[1], Nuria Porta[1], Wei Yuan[1], Suzanne Carreira[1], and Johann S. de Bono[1,2]

ABSTRACT

Purpose: Cyclin-dependent kinase 12 (CDK12) aberrations have been reported as a biomarker of response to immunotherapy for metastatic castration-resistant prostate cancer (mCRPC). Herein, we characterize CDK12-mutated mCRPC, presenting clinical, genomic, and tumor-infiltrating lymphocyte (TIL) data.

Experimental Design: Patients with mCRPC consented to the molecular analyses of diagnostic and mCRPC biopsies. Genomic analyses involved targeted next-generation (MiSeq; Illumina) and exome sequencing (NovaSeq; Illumina). TILs were assessed by validated immunocytochemistry coupled with deep learning–based artificial intelligence analyses including multiplex immunofluorescence assays for CD4, CD8, and FOXP3 evaluating TIL subsets. The control group comprised a randomly selected mCRPC cohort with sequencing and clinical data available.

Results: Biopsies from 913 patients underwent targeted sequencing between February 2015 and October 2019. Forty-three patients (4.7%) had tumors with CDK12 alterations. CDK12-altered cancers had distinctive features, with some revealing high chromosomal break numbers in exome sequencing. Biallelic CDK12-aberrant mCRPCs had shorter overall survival from diagnosis than controls [5.1 years (95% confidence interval (CI), 4.0–7.9) vs. 6.4 years (95% CI, 5.7–7.8); hazard ratio (HR), 1.65 (95% CI, 1.07–2.53); $P = 0.02$]. Median intratumoral $CD3^+$ cell density was higher in CDK12 cancers, although this was not statistically significant (203.7 vs. 86.7 cells/mm^2; $P = 0.07$). This infiltrate primarily comprised of $CD4^+FOXP3^-$ cells (50.5 vs. 6.2 cells/mm^2; $P < 0.0001$), where high counts tended to be associated with worse survival from diagnosis (HR, 1.64; 95% CI, 0.95–2.84; $P = 0.077$) in the overall population.

Conclusions: CDK12-altered mCRPCs have worse prognosis, with these tumors surprisingly being primarily enriched for $CD4^+FOXP3^-$ cells that seem to associate with worse outcome and may be immunosuppressive.

See related commentary by Lotan and Antonarakis, p. 380

Introduction

Cyclin-dependent kinase 12 (CDK12) is a transcription-associated CDK, which forms a heterodimeric complex with cyclin K (CycK), implicated in DNA repair (DDR), splicing, and differentiation (1–6). CDK12 maps on chromosome 17q12 RNA and generates two mRNA splice isoforms, differing only in the last exon, with both having a central kinase region flanked by large N- and C-terminal extensions with arginine-serine–rich (RS) domains (3). Recent genomic analyses of primary (7–11) and metastatic castration-resistant prostate cancer (mCRPC; refs. 11–15) have identified recurrent, deleterious CDK12 alterations in 2%–4% of primary prostate cancers (9, 11) and in 4.7%–11% of mCRPCs (11, 14, 15). Integrative genomic analysis of 360 mCRPC samples has demonstrated that CDK12-mutated prostate cancer is genetically, transcriptionally, and phenotypically distinct from tumors with homologous recombination repair defects and mismatch repair deficiency (MMRd; ref. 16), being reported to have innumerable tandem duplications (TD) and genomic rearrangements, high neoantigen burdens, and increased tumor-infiltrating lymphocytes (TIL; ref. 16). This is postulated to confer a vulnerability to immunotherapy similar to cancers with MMRd (16, 17), with this genomic profile probably also acquiring immune cell evasive strategies to allow tumor growth (18–20).

Understanding the clinical, molecular, and immune characteristics of these tumors is critically important for the development of successful clinical therapeutic strategies for this disease subclass (20–22). Herein, we characterize *CDK12*-mutated prostate cancer, with both biallelic and monoallelic aberrations, describing their genomic, clinical, histopathologic, and immune infiltrate features.

Materials and Methods

Patient population

This retrospective study included patients with mCRPC who consented for molecular characterization of their prostate cancer biopsies at The Institute of Cancer Research (Sutton, London, United Kingdom). Consent was obtained either within a Royal Marsden Hospital (Sutton, London, United Kingdom)-specific protocol (Ethics Review Committee reference no. 04/Q0801/60) and/or the phase II trial TOPARP-B (ClinicalTrials.gov, NCT01682772). These studies were conducted in accordance with the Declaration of Helsinki. Both studies allowed acquisition, whenever possible, of a mCRPC biopsy and the diagnostic hormone-sensitive prostate cancer (HSPC) biopsy.

[1]The Institute of Cancer Research, Sutton, London, United Kingdom. [2]The Royal Marsden NHS Foundation Trust, Sutton, London, United Kingdom. [3]Vall d'Hebron Institute of Oncology (VHIO) and Vall d'Hebron University Hospital, Barcelona, Spain.

Note: Supplementary data for this article are available at Clinical Cancer Research Online (http://clincancerres.aacrjournals.org/).

P. Rescigno and B. Gurel contributed equally to this article.

Corresponding Author: Johann S. de Bono, The Institute of Cancer Research, London SM2 5NG, United Kingdom. Phone: 4420-8722-4028; Fax: 4420-8642-7979; E-mail: johann.de-bono@icr.ac.uk

Clin Cancer Res 2021;27:566–74

doi: 10.1158/1078-0432.CCR-20-2371

Translational Relevance

Prostate cancers harboring cyclin-dependent kinase 12 alterations have a worse prognosis and are enriched primarily in $CD4^{+}FOXP3^{-}$ tumor-infiltrating lymphocytes that associate with a worse prognosis.

Demographic and clinical data for each patient were collected from the hospital electronic patient record or the clinical trial database. Clinical outcomes included overall survival (OS) from diagnosis, OS from castration resistance, and time to CRPC, respectively, defined as the time between diagnosis of prostate cancer and death or last follow-up, between castration resistance and death or last follow-up, and between diagnosis and castration resistance. Furthermore, time-on-treatment with abiraterone/enzalutamide (whichever came first) was investigated separately before and after treatment with docetaxel.

Tumor tissue samples

Formalin-fixed, paraffin-embedded (FFPE) prostate cancer tissue was obtained from prostate needle biopsies, transurethral resections of the prostate, prostatectomies, or prostate cancer metastases within bone (bone marrow trephine), lymph node, soft tissue, or visceral metastases (needle biopsies). A subset of patients had matching, same patient, primary tissue and CRPC biopsies available. All tissue blocks were freshly sectioned, and tumor content was confirmed by examination of hematoxylin and eosin–stained samples sections by a trained pathologist (B. Gurel).

Next-generation sequencing

Targeted next-generation sequencing (NGS) was performed on diagnostic and mCRPC samples. DNA was extracted from FFPE blocks positive for tumor content using the FFPE Tissue DNA Kit (Qiagen) and quantified with the Quant-iT High-sensitivity PicoGreen Double-stranded DNA Assay Kit (Invitrogen). The Illumina FFPE QC Kit (WG-321-1001) was used for DNA quality control tests according to the manufacturer's protocol. Libraries for targeted NGS were constructed from 40 ng of DNA using a customized panel (GeneRead DNAseq Mix-n-Match Panel v2; Qiagen) covering 6,025 amplicons across 113 genes. Libraries were run using the MiSeq Sequencer (Illumina). FASTQ files were generated using the Illumina MiSeq Reporter v2.5.1.3. Sequence alignment and mutation calling were performed using BWA tools and the Genome Analysis Toolkit (GATK) variant annotator by the Qiagen GeneRead Targeted Exon Enrichment Panel Data Analysis web portal. Biallelic alterations in *CDK12* were prospectively defined as (i) a deleterious mutation with LOH at the wild-type allele, (ii) copy-number loss (homozygous deletion), and (iii) ≥2 *CDK12* deleterious genomic alterations in a given sample. Mutations with >5% allele frequency were reported.

Exome sequencing and copy-number break analysis

Libraries for whole-exome sequencing were performed using Kapa Hyper Plus Library Prep Kits and the Agilent SureSelectXT V6 Target Enrichment Kit. Paired-end sequencing was performed using the NovaSeq 6000 S2 Flow Cell (2 × 100 cycles, Illumina). FASTQ files were generated from the sequencer's output using Illumina bcl2fastq2 Software (v.2.17.1.14, Illumina) with the default chastity filter to select sequence reads for subsequent analyses. All reads were aligned to the human genome reference sequence (GRCh37-hg19) using the BWA-MEM algorithm (v. 0.7.12). Picard tools (v.2.8.2) were used to mark PCR duplicates and to calculate sequencing metrics for quality control check. The GATK (v. 3.5-0) was applied to realign local insertions/deletions (indels), recalibrate base scores, and identify point mutations, small insertions, and deletions. Somatic point mutations and indels were called using MuTect2 by comparing tumor DNA with germline DNA control. Copy-number estimation was obtained through a modified ASCAT2 package. Copy Number Alterations (CNA) segmentation file was used to define the CNA breakpoint when there was a change of segment and/or CNA.

Immunohistochemistry (IHC)

Three-micron-thick sections from FFPE tissue blocks were obtained using a microtome, floated in a water bath, and mounted in Superfrost slides. Slides were baked and dried overnight at 37°C. CD3 IHC was performed using a rabbit anti-CD3 antibody (#A0452; polyclonal; Dako; Agilent Technologies) and an automated Staining Platform (Bond-RX, Leica Microsystems). Antigen retrieval was achieved by using Bond Epitope Retrieval Solution 1 (#AR9961, Leica Biosystems) for 30 minutes prior to incubation with anti-CD3 antibody (1:150 dilution) for 15 minutes at room temperature. The reaction was visualized using the Bond Polymer Refine Kit (#DS9800, Leica Biosystems). Antibody specificity was confirmed in human appendix and prostate tissues (positive controls) and LNCaP cell pellets (negative control).

PTEN and ATM protein expression studies were conducted as described previously (23, 24).

Nuclear staining (and cytoplasmic staining for PTEN) was semi-quantitatively assessed using an H-score (3× % of strongly stained cells and 2× the % of moderately stained cells, and the % of weakly stained cells, for a range of 0–300). Cases were considered as PTEN or ATM loss if they had an H-score ≤ 10.

Slide digitization and computer-assisted image analysis for IHC

CD3 IHC-stained slides were scanned at high resolution (200×) using the ZEISS Axio Scan.Z1 Digital Slide Scanner (Carl Zeiss AG). The digitized slides were then analyzed with the HALO image analysis suite (Indica Labs). A supervised machine learning algorithm was trained to recognize prostate cancer foci and surrounding stroma. Color deconvolution for DAB and hematoxylin stains was performed, cell recognition and nuclear segmentation were optimized for hematoxylin stain, and recognition of CD3 staining was optimized for the membranous and cytoplasmic compartments. The analysis algorithm was adjusted to provide optical density data for intensity of CD3 membranous and cytoplasmic staining in the automatically annotated tumor and stromal regions. A threshold was set to categorize each detected cell into CD3 positive or negative. The number of intratumoral and stromal CD3-positive cells was then divided by the total area of prostate tumor and stroma, respectively, providing intratumoral and stromal CD3 density values ($CD3^{+}/mm^{2}$) for each sample. Each stained sample was also visually assessed and assigned an intratumoral and stromal chronic inflammation score, using a modified version of the histopathologic classification system developed by Nickel and colleagues (25).

Multiplex immunofluorescence assay

Intratumoral TILs were determined by immunofluorescence (IF) for T-cell subpopulations as described previously (26). Briefly, multiplex IF staining was performed on 3-μm-thick FFPE tissue sections using an automated staining platform (BOND RX, Leica Microsystems). Antigen retrieval was achieved using BOND Epitope Retrieval Solution 2 (#AR9640, Leica Microsystems). Endogenous peroxidase

was inactivated in 3% H_2O_2. Tissue sections were incubated with antibodies against CD4 (#ab133616, clone EPR6855, 1:100, Abcam) and CD8 (#M7103, clone C8/144B, 1:200, Dako, Agilent Technologies), and detected with Alexa Fluor 555–conjugated IgG (H+L) goat anti-rabbit (#A21429, Invitrogen) and Alexa Fluor 488–conjugated IgG (H+L) goat anti-mouse (#A-11029, Invitrogen) secondary antibodies, respectively. Endogenous biotin was blocked with Avidin/Biotin Blocking Kit according to the manufacturer's protocol (#ab64212, Abcam). Next, tissue sections were incubated with antibodies against FOXP3 conjugated to biotin (#13-4777-82, clone 236A/E7, 1:100, eBioscience) and pan-cytokeratin (PanCK) conjugated to Alexa Fluor 647 (#4528S, clone C11, 1:100, Cell Signaling Technology), followed by streptavidin peroxidase (horseradish peroxidase) (#K5001, Dako, Agilent Technologies) and TSA Coumarin Detection System (#NEL703001KT, Akoya Biosciences). Nuclei were counterstained with DRAQ 7 (#DR71000, BioStatus) and tissue sections were mounted with ProLong Gold Antifade Reagent (#P36930, Molecular Probes).

Slides were scanned using the Vectra Automated Multispectral Imaging System (Akoya Biosciences) and analyzed using inForm v2.2.1 (Akoya Biosciences). Tissue and nuclear cell segmentation were performed using methods described previously (1). TIL phenotype determination was based on staining for CD8, CD4, and FOXP3, and were separated into bins as follows: $CD8^+$, $CD4^+FOXP3^+$, and $CD4^+FOXP3^-$ T cells. Quantification of the immune cell densities are presented as number of cells per mm^2.

Statistical analysis

In this analysis, the prevalence of *CDK12* aberrations observed in our cohort was reported. In a subset of patients with available clinical ($n = 36$, 28 biallelic and eight monoallelic) and TIL data ($n = 24$, 17 biallelic and seven monoallelic), tumors with *CDK12* aberrations were compared with a control group that comprised a random selection of patients concurrently sequenced at our institution without such aberrations or mismatch repair alterations. Comparison of lymphocyte infiltration between *CDK12* biallelic cases, *CDK12* monoallelic cases, and controls was performed using a *t* test after density per mm^2 was $\log_{10}$ transformed, whereas Wilcoxon rank-sum test assessed differences between diagnostic and mCRPC samples in *CDK12* cases. Wilcoxon rank-sum test was also used for copy-number breaks (CNB) comparison between *CDK12* biallelic cases, *CDK12* monoallelic cases, and controls. Kaplan–Meier estimator and Cox regression models were used for time-to-event analyses comparing controls and biallelic *CDK12* cases only. In a sensitivity analysis, all time-to-event analyses were repeated with mono- and biallelic *CDK12* cases being pooled into one group and compared with the control group. The significance level was set to 5% for all analyses and there was no multiplicity adjustment made as to the exploratory nature of this work. Analyses were carried out with R version 3.6.2.

Results

CDK12-altered prostate cancers

Between March 2015 and October 2019, 913 patients with prostate cancer were analyzed by targeted NGS after passing quality control. All patients had a histologic diagnosis of prostate cancer and either diagnostic tissue and/or a mCRPC biopsy sample available for analysis; the patient characteristics and their treatment histories are described in **Table 1** and Supplementary Table S1. We identified 43 patients with potentially pathogenic alterations of *CDK12* (4.7%), of which 31 (3.4%) had biallelic genomic aberrations. One tumor had a concomitant MSH6 somatic mutation with associated MSH6 loss of expression on *IHC* and was not included in subsequent analyses, being deemed to be an MMRd prostate cancer. The remaining 11 patients were considered to have monoallelic *CDK12* alterations (Supplementary Fig. S1).

For the 31 biallelic cases identified, a total of 34 diagnostic and mCRPC samples were sequenced by NGS; 3 patients had matched

Table 1. Patients characteristics.

	Overall	Control	Monoallelic	Biallelic	*P*
n	180	144	8	28	
Age at diagnosis [median (IQR)]	61.0 (56.0–64.2)	61.0 (55.8–64.0)	59.0 (55.0–63.5)	62.5 (60.0–65.0)	0.401[a]
T group (%)					0.281[b]
T1	2 (1.1)	1 (0.7)	1 (12.5)	0 (0.0)	
T2	20 (11.1)	18 (12.5)	0 (0.0)	2 (7.1)	
T3	76 (42.2)	57 (39.6)	4 (50.0)	15 (53.6)	
T4	34 (18.9)	26 (18.1)	2 (25.0)	6 (21.4)	
TX	48 (26.7)	42 (29.2)	1 (12.5)	5 (17.9)	
T3/4 = yes (%)	110 (83.3)	83 (81.4)	6 (85.7)	21 (91.3)	0.623[b]
N (%)					0.197[b]
N0	42 (36.8)	28 (33.3)	5 (83.3)	9 (37.5)	
N1	65 (57.0)	51 (60.7)	1 (16.7)	13 (54.2)	
N2	7 (6.1)	5 (6.0)	0 (0.0)	2 (8.3)	
N1/2 = yes (%)	72 (63.2)	56 (66.7)	1 (16.7)	15 (62.5)	0.059[b]
M = M1 (%)	96 (56.5)	76 (56.3)	2 (28.6)	18 (64.3)	0.231[b]
Total Gleason score (G) [median (IQR)]	9.0 (7.0–9.0)	8.0 (7.0–9.0)	9.0 (7.8–9.0)	9.0 (9.0–9.0)	<0.001[a]
G ≤ 7 vs. G > 8 = yes (%)	117 (72.2)	84 (66.1)	6 (75.0)	27 (100.0)	<0.001[b]
PSA at diagnosis mcg/L [median (IQR)]	63.0 (15.4–176.1)	53.5 (10.9–162.0)	106.0 (34.5–137.0)	72.0 (25.5–229.2)	0.449[a]
Prostatectomy Y/N = yes (%)	22 (12.2)	18 (12.5)	2 (25.0)	2 (7.1)	0.318[b]
Radiotherapy Y/N = yes (%)	67 (37.2)	57 (39.6)	2 (25.0)	8 (28.6)	0.450[b]

Abbreviations: IQR, interquartile range T size and extent of the main tumor; M, presence of metastatic disease; N, presence of nodal disease.
[a]Kruskal–Wallis test.
[b]Fisher exact test.

primary and metastatic samples available for analyses, which were concordant with the presence of the same *CDK12* genomic alterations. The biallelic group comprised of 11 missense alterations, 13 nonsense alterations, 32 frameshift mutations or indels, and two splice site mutations. We discovered a *CDK12* deep deletion on copy-number analysis in one case (**Fig. 1A**; Supplementary Table S2). The majority of these aberrations were truncating mutations, predominantly located in the region between the amino terminus and the kinase domain or within the kinase domain, whereas the missense mutations were predominantly clustered in the *CDK12* kinase domain. Two patients had three *CDK12* aberrations, including V463G, one of the missense mutations not located in the kinase domain (lollipop plot shown in **Fig. 1A**).

Beyond the MMRd cancer with a concomitant *CDK12* deleterious alteration, we identified multiple prostate cancers with biallelic *CDK12* deleterious alterations contemporaneously harboring other DDR defects (**Fig. 1B**). The prostate cancer with *CDK12* deep deletion also had an *ATM* alteration and ATM loss detected by IHC. Other samples presented with pathogenic *PALB2 alteration (I265Tfs*12 in diagnostic and CRPC biopsies), BRCA2 (S744*) and CHEK2 (L464fs*16) mutations, FANCA deep deletion*, and FANCL frameshift mutation (T372Ifs*2). Other alterations in *CDK12* biallelic tumors included *PTEN mutations, the androgen receptor (AR) L702H point mutation, PIK3CA activating mutation (E545K), and SPOP alterations* (Supplementary Table S2). We had IHC data for PTEN and ATM available, respectively, for 16 and 17 of the 31 *CDK12* biallelic cases. Interestingly, none of the cancers with biallelic *CDK12* alterations had PTEN loss by IHC; conversely, four of the biallelic *CDK12* tumors (4/17, 23.5%) had ATM loss, detected by IHC.

Clinical outcomes of prostate cancer with *CDK12* alterations

Clinical data were available for 36 of the 42 patients with *CDK12* aberrations (28 biallelic and eight monoallelic) and were compared with the data of 144 controls. Patient characteristics and treatment histories are described in **Table 1** and Supplementary Table S1. The two groups were balanced for age, staging, and presence of metastatic disease, as well as for PSA levels and initial treatment received. However, *CDK12* tumors had higher Gleason scores at diagnosis ($P < 0.001$). Biallelic *CDK12* cases experienced worse survival than the control group with a median OS from diagnosis, 6.4 years [95% confidence interval (CI), 5.7–7.8] for the control group and 5.1 years (95% CI, 4.0–7.9) for the biallelic *CDK12* group (HR, 1.65; 95% CI, 1.07–2.53; $P = 0.02$). Similar results were obtained when monoallelic and biallelic cases were combined into one group and compared with controls (HR, 1.50; 95% CI, 1.02–2.20; $P = 0.04$; **Fig. 2A** and **B**) and when OS was estimated from the date of CRPC (**Fig. 2C** and **D**). However, in the multivariable analysis, *CDK12* mutational status was no longer independently prognostic (HR, 0.94; 95% CI, 0.6–1.6; $P = 0.81$; Supplementary Table S3). Median time to CRPC diagnosis was not different between biallelic and control cohorts, being 1.9 years (95% CI, 1.4–2.6) in the control group and 2.2 years (95% CI, 1.5–2.7) in the biallelic *CDK12* group (HR, 1.25; 95% CI, 0.82–1.91; $P = 0.3$; Supplementary Fig. S2A). Almost all patients had received docetaxel chemotherapy and abiraterone/enzalutamide; 61% of patients in the

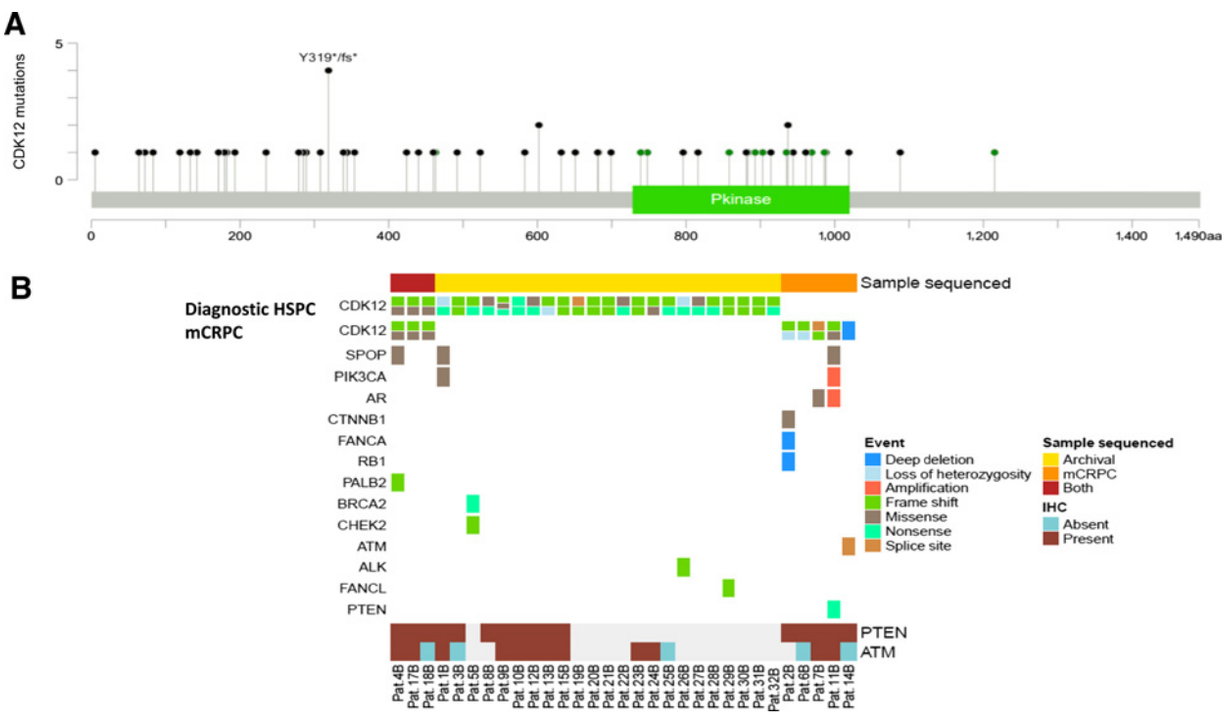

Figure 1.

A, Lollipop plot depicting mutations in *CDK12* in this prostate cancer cohort with biallelic alterations ($n = 31$); missense mutations are depicted in green and frameshift and nonsense mutations in black. **B,** OncoPrint figure representing *CDK12* mutations for the biallelic tumors in HSPC and mCRPC samples (top). Concomitant alterations in other DDR genes and other relevant pathways in prostate cancer, detected on targeted and exome sequencing in diagnostic and/or mCRPC samples (middle). The available IHC data for PTEN and ATM for the samples sequenced (bottom). PTEN and ATM data were, respectively, available for 16 and 17 samples of the 31 *CDK12* biallelic cases. Gray boxes indicate sample with no available PTEN or ATM results by IHC.

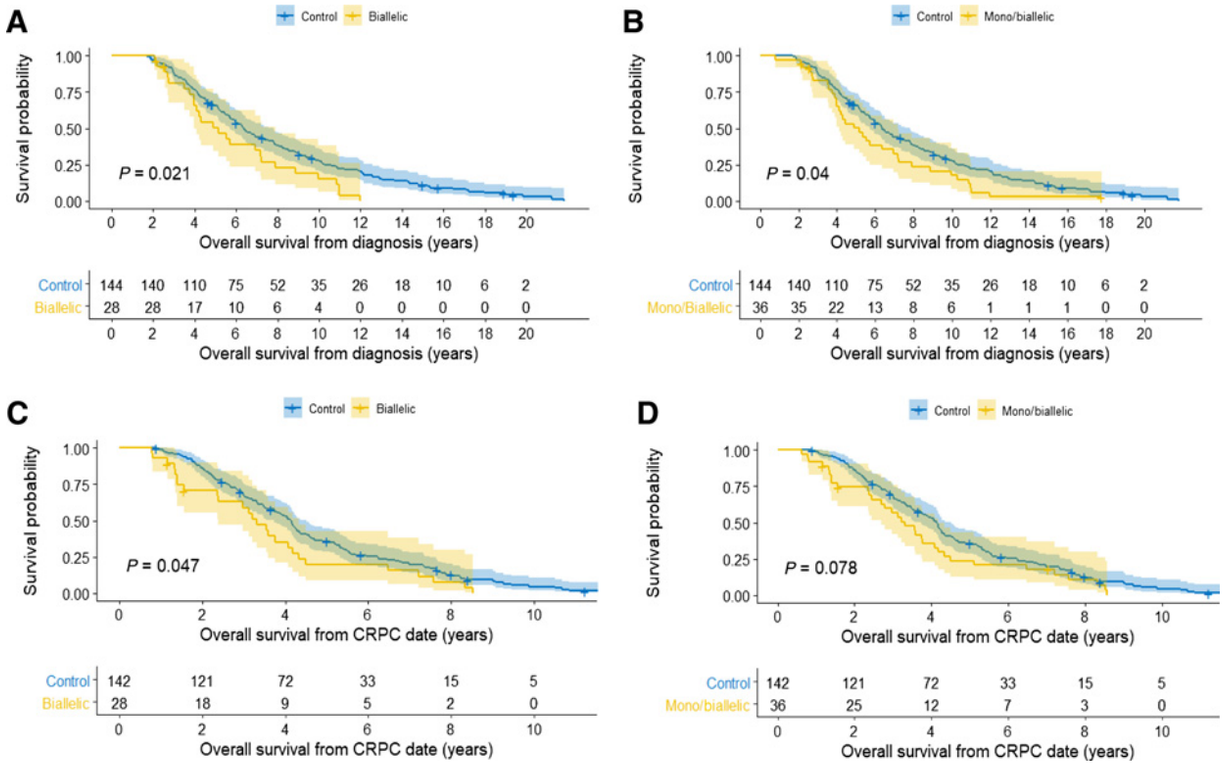

Figure 2.

Survival curves. **A,** Kaplan–Meier curves for OS from date of diagnosis. *CDK12* biallelic-mutated cases in yellow and controls in blue. **B,** Kaplan–Meier curves for OS from date of diagnosis. *CDK12* biallelic- and monoallelic-mutated cases in yellow and controls in blue. **C,** Kaplan–Meier curves for OS from date of CRPC diagnosis. *CDK12* biallelic-mutated cases in yellow and controls in blue. **D,** Kaplan–Meier curves for OS from date of CRPC diagnosis. *CDK12* biallelic- and monoallelic-mutated cases in yellow and controls in blue.

control group received cabazitaxel, whereas only 36% patients in the combined mono/biallelic *CDK12* group received cabazitaxel (Supplementary Table S1). There was no statistically significant difference in time on abiraterone/enzalutamide treatment between the groups, with median duration of treatment in the pre-docetaxel setting being 7.6 months (95% CI, 6.0–9.3) in the control group and 8.2 months (95% CI, 4.7, NA) in the biallelic *CDK12* group (HR, 1.07; 95% CI, 0.58–2.11; $P = 0.75$), with similar findings in the post-docetaxel setting (Supplementary Fig. S2B and S2C) and when monoallelic and biallelic cases were combined into one group (data not shown).

Exome sequencing data

Overall, of the 913 patients with prostate cancer evaluated by targeted NGS, 211 patients (diagnostic = 93 and CRPC = 118) had samples suitable for exome sequencing including 26 samples harboring *CDK12* genomic aberrations, 23 of which were biallelic and three monoallelic. Although 73% of the *CDK12*-aberrant cases (19/26) had CNB values higher than the median, which was 513 (Q1, 405.5 and Q3, 617.5), only 10 of the 26 (38.5%) *CDK12*-aberrant cases were above the CNB top quartile (**Fig. 3A**). In general, however, *CDK12* tumors had significantly higher CNBs than the controls ($P = 0.01$; **Fig. 3B**).

TIL analyses

For the analysis of intratumor $CD3^+$ TIL density (D-TIL), there were 122 samples for controls as well as 17 samples with biallelic *CDK12* alterations and seven monoallelic *CDK12* alteration cases (total $N = 146$; **Fig. 4A** and **B**). Median intratumoral total $CD3^+$ cell density was higher in *CDK12* biallelic loss samples than in controls, although this was not statistically significant (203.7 vs. 86.7 $CD3^+/mm^2$; $P = 0.073$; **Fig. 4B**). Two of the *CDK12* biallelic loss prostate cancer cases had more than 1,200 $CD3^+$ cells per mm^2, which was above the 90% centile (**Fig. 4A**); however, multiple samples with biallelic *CDK12* aberrations had $CD3^+$ counts that were below the median. D-TIL was not statistically different between diagnostic and mCRPC samples for all *CDK12* cases (Supplementary Fig. S3). Interestingly, there was no association found in our analyses between CNBs and D-TIL, neither in diagnostic nor CRPC samples. The samples with the highest $CD3^+$ density also had the highest $CD4^+$ and $CD8^+$ infiltrates. The two samples with the highest $CD3^+$ density had modest CNB scores of 613 and 600 (just above the median of 513).

We next quantified D-TILs, on the basis of T-cell subtypes (**Fig. 5A** and **B**; Supplementary Fig. S4A–S4C); tissue sites included prostate tissue ($n = 9$), lymph node biopsies ($n = 31$), bone ($n = 10$), liver ($n = 1$), and soft tissue metastases ($n = 1$; Supplementary Table S4). In the overall population, total $CD3^+$ cell numbers were correlated with $CD4^+FOXP3^-$ ($R = 0.51$; $P < 0.001$) and $CD8^+$ cell numbers ($R = 0.45$; $P < 0.001$; **Fig. 5A**). Moreover, our analyses revealed that *CDK12* cancers were significantly enriched for $CD4^+FOXP3^-$ cells (median $CD4^+FOXP3^-/mm^2$ 50.5 in *CDK12* biallelic cases vs. 6.2 in controls; $P < 0.001$), with a higher CD4/CD8 ratio (r) compared with controls (CD4/CD8 r = 1.22 for *CDK12* biallelic cases vs. 0.4 for controls),

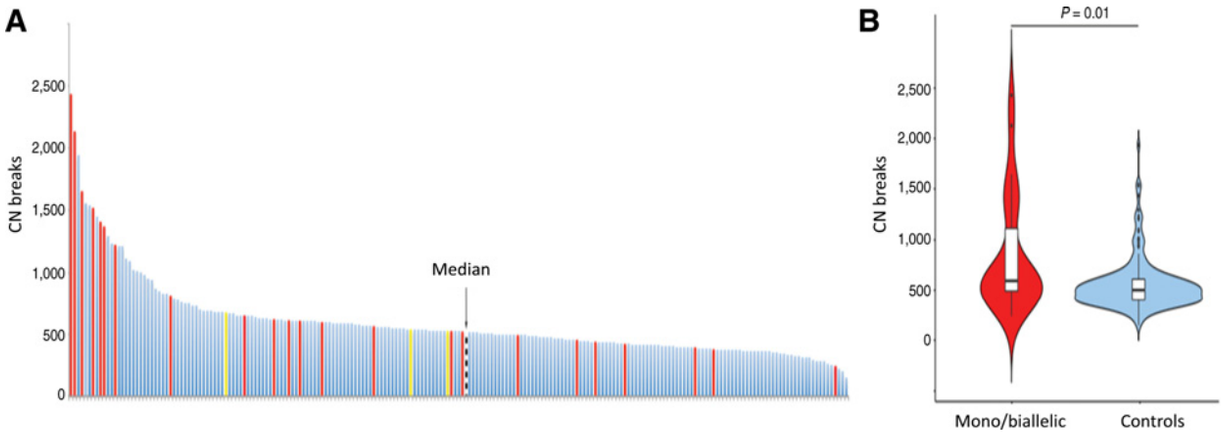

Figure 3.
Genomic analyses. **A,** CNBs determined from exome sequencing data in $n = 211$ patients. *CDK12* biallelic mutation cases ($n = 23$) in red, monoallelic cases ($n = 3$) in yellow, and cancers with no *CDK12* alterations (controls) in blue. The black line indicates the median number of CNBs (median = 513) in the whole cohort. **B,** Violin plot depicting CNB numbers in *CDK12*-mutated cases (red) and in controls (blue).

without significantly higher $CD8^+$ or $CD4^+FOXP3^+$ cells (**Fig. 5B**). Higher $CD4^+FOXP3^-$ infiltration appeared to be associated with shorter OS (HR, 1.64; 95% CI, 0.95–2.84; $P = 0.077$), with similar trends for $CD4^+FOXP3^+$ and $CD8^+$ cells (HR, 1.14; 95% CI, 0.73–1.76; $P = 0.6$ and HR, 1.42; 95% CI, 0.94–2.16; $P = 0.0967$, respectively).

Discussion

Deleterious *CDK12* mutations have been reported in multiple tumor types, but are not common, although they may have special clinical importance in view of their immunogenomic properties. A subset of mCRPC has deleterious *CDK12* aberrations (16, 27, 28), resulting in characteristic genomic profiles with innumerable focal TDs, gene fusions, and neoantigens (16, 27). These prostate cancer *CDK12* alterations, like MMRd, have been postulated to represent a predictive biomarker of response to immunotherapy (17), making their study of huge interest (29, 30). Our analysis is arguably one of the largest integrated efforts interrogating their genomic, pathologic, and clinical characteristics, and also investigating their TIL landscape.

We confirm that approximately 5% of mCRPCs have *CDK12* deleterious aberrations (11, 16), although fewer (3.4%) are definitely biallelic with the majority being frameshift or nonsense mutations and a small minority single-nucleotide aberrations of the kinase domain with a high likelihood of impact on protein function. Interestingly, these alterations were invariably present at diagnosis in matched same patient HSPC and mCRPC biopsies, suggesting that they are clonal events. Exome analyses have identified a specific genomic pattern of *CDK12*-aberrant cancers characterized by a high number of CNBs, and this highly fragmented genome has been shown to be correlated with a tandem duplicator phenotype (16). In our analysis, although high CNBs were characteristic of these tumors, not all prostate cancers with biallelic *CDK12* alterations had this genomic signature, indicating that this may not be useful as the sole test to identify this subset. However, in

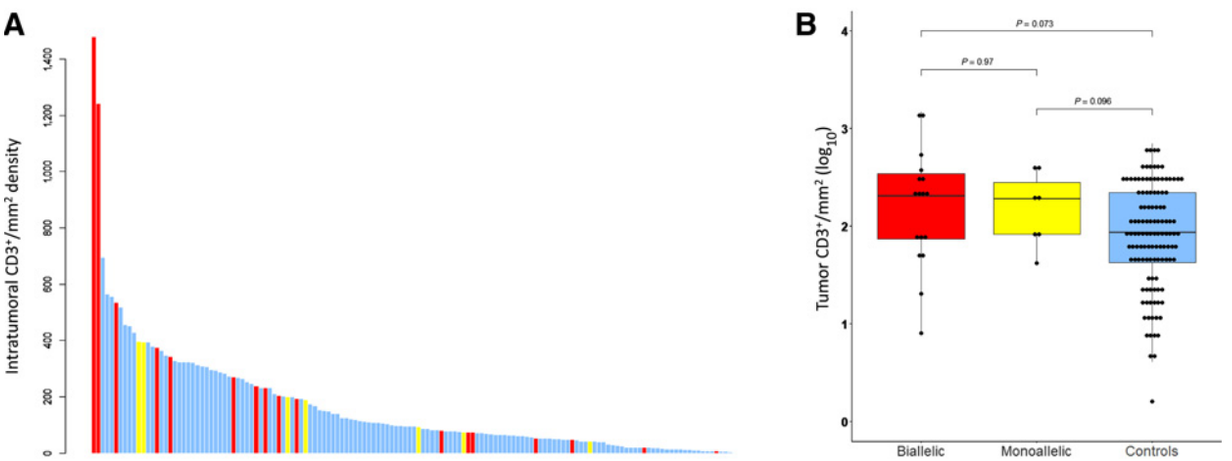

Figure 4.
TILs analyses. **A,** Intratumoral $CD3^+$ TILs per mm^2. Bar chart depicting intratumoral $CD3^+/mm^2$ density (*y*-axis) in *CDK12* biallelic cases (red), monoallelic cases (yellow), and controls (blue). **B,** Box and whisker plot of log_{10}-transformed intratumoral $CD3^+$ cell density per mm^2 depicting *CDK12* biallelic cases (red), monoallelic cases (yellow), and control cases (blue).

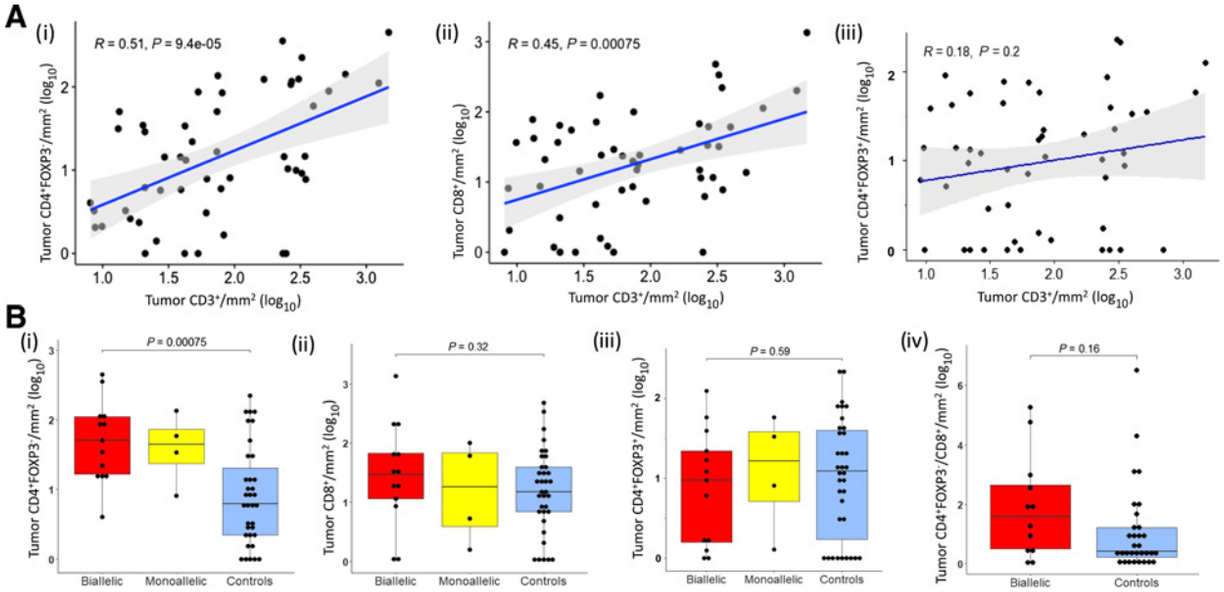

Figure 5.

TIL subset analyses. **A,** Scatter plots depicting associations between log-transformed $CD3^+$ cells/mm^2 TILs and $CD4^+FOXP3^-$ cells/mm^2 (i), $CD3^+$ cells/mm^2 and $CD8^+$cells/mm^2 (ii), and $CD3^+$ cells/mm^2 and $CD4^+FOXP3+$cells/mm^2 (iii). **B,** Box and whisker plots representing intratumoral infiltrate density as log_{10}-transformed $CD4^+FOXP3^-$ cells/mm^2 (i), $CD8^+$cells/mm^2 (ii), $CD4^+$ $FOXP3^+$cells/mm^2 (iii) in *CDK12* biallelic (red), monoallelic (yellow), and control cases (blue); and (iv) tumor $CD4^+FOXP3^-/CD8^+$ ratio between biallelic cases (red) and controls (blue).

keeping with the PROfound olaparib phase III genomic analyses data, we did observe concomitant mutations in other DDR genes in CDK-altered tumors including *PALB2, BRCA2, FANCA, ATM*, and *MSH6* and in *AR, PTEN*, and *PI3K/AKT* pathway genes, with 23.5% of these cancers presenting concomitant ATM loss, but no PTEN loss by IHC (31). We also showed that prostate cancer with *CDK12* biallelic alterations associate with higher Gleason scores and shorter survival from diagnosis, although we did not observe any differences in outcome on abiraterone/enzalutamide treatment, which has been previously reported, maybe due to the retrospective nature of our investigation (29, 30).

We also show for the first time that prostate cancer with biallelic *CDK12* aberrations are predominantly enriched for $CD4^+FOXP3^-$ cells with these tumors surprisingly not having significantly higher $CD4^+FOXP3^+$ or $CD8^+$ TILs compared with controls. Interestingly, multiple studies have reported on immunosuppressive $CD4^+FOXP3^-$ TIL subsets (32, 33), with some of these cells being reported to express high PD-1 and being able to inhibit cytotoxic T-cell function in a PD-1/PD-L1–dependent fashion as well as limit immunotherapy antitumor activity (32). The data, herein, suggest that $CD4^+FOXP3^-$ cells, which *CDK12*-altered prostate cancer seem to be enriched for, might have an immunosuppressive role, associating with worse survival and might be relevant to immunotherapy trials as a biomarker of interest (30, 34, 35).

We acknowledge that significant limitations of our data include the fact that this was a single-institution retrospective study, and that, while we screened almost a thousand patients, our *CDK12* analyses are based on a relatively small cohort, even though this comprises one of the largest studies of mCRPC subjects. Furthermore, we acknowledge that more effort is now needed to elucidate why not all prostate cancers with biallelic *CDK12* alterations have the TD signature, and studies need to evaluate whether monoallelic loss can result in any biological relevance perhaps due to haploinsufficiency and a gene dose effect. Moreover, further studies to characterize the $CD4^+FOXP3^-$ TIL subset are now crucial to drive therapeutic advances for this subset.

In conclusion, our data indicate that biallelic *CDK12* aberrations in prostate cancer are associated with higher Gleason grade and poorer prognosis, and are infiltrated by $CD4^+FOXP3^-$ T lymphocytes that appear to be associated with worse outcome and are likely to be immunosuppressive, with this being relevant to immunotherapy approaches.

Authors' Disclosures

J. Mateo reports grants, personal fees, and nonfinancial support from AstraZeneca (advisory board, grant to institution as principal investigator, speakers bureau), grants from Pfizer Oncology (grant to institution as principal investigator), personal fees and nonfinancial support from Clovis Oncology (advisory board, material and samples for research), Janssen (advisory board, travel to conference support, speakers bureau), and personal fees from Amgen (advisory board), Roche (advisory board), Merck-MSD (advisory board), and Astellas (Speakers bureau) outside the submitted work. A. Sharp reports personal fees from Sanofi (travel), Roche-Genentech (travel), and Astellas (speaker) outside the submitted work and reports employment with The Institute of Cancer Research (ICR), which has a commercial interest in abiraterone. W. Yuan reports receiving a meeting travel grant from Jilin Huarui Gene Technology Ltd. M.D. Fenor de la Maza has received grants and fees from "Fundación Cris contra el Cáncer"; travel fees from Astellas, AstraZeneca, Pfizer, Pierre Fabre, Roche, Bristol Meiers Squibb, Novartis, MSD, Janssen, and Bayer Pharmamar; and personal fees from Janssen, Pierre Fabre, and Roche outside the submitted work. J.S. de Bono reports grants, personal fees, and other from AstraZeneca (honorarium, travel expenses) during the conduct of the study, grants, personal fees, and other from Astellas (honorarium, travel expenses), Bayer (honorarium, travel expenses), BioXCell Therapeutics (honorarium, travel expenses), CellCentric (honorarium, travel expenses), Daiichi Sankyo (honorarium, travel expenses), Genentech/Roche (honorarium, travel expenses), Genmab (honorarium, travel expenses), GlaxoSmithKline (honorarium, travel expenses), Janssen (honorarium, travel expenses), Merck Serono (honorarium, travel expenses), Merck Sharp & Dohme (honorarium, travel expenses), Menarini/Silicon Biosystems (honorarium, travel expenses), Orion (honorarium, travel expenses), Pfizer (honorarium, travel expenses), Sanofi Aventis (honorarium, travel expenses), Sierra Oncology (honorarium, travel expenses), Taiho (honorarium, travel expenses), and Vertex Pharmaceuticals (honorarium, travel

expenses), personal fees and other from Boehringer Ingelheim (honorarium, travel expenses), Eisai (honorarium, travel expenses), and Qiagen (honorarium, travel expenses) outside of the submitted work, and is listed as an inventor on a patent regarding PARP inhibition in DNA repair defective cancers owned by ICR and licensed to AstraZeneca. No disclosures were reported by the other authors.

Authors' Contributions

P. Rescigno: Conceptualization, data curation, investigation, visualization, writing-original draft, writing-review and editing. **B. Gurel:** Conceptualization, data curation, formal analysis, investigation, visualization, methodology, writing-original draft. **R. Pereira:** Data curation. **M. Crespo:** Formal analysis, investigation, visualization, methodology, writing-review and editing. **J. Rekowski:** Software, formal analysis, investigation, visualization, methodology, writing-review and editing. **M. Rediti:** Data curation. **M. Barrero:** Data curation. **J. Mateo:** Data curation. **D. Bianchini:** Data curation. **C. Messina:** Data curation. **M.D. Fenor de la Maza:** Data curation. **K. Chandran:** Data curation. **J. Carmichael:** Data curation. **C. Guo:** Data curation. **A. Paschalis:** Data curation. **A. Sharp:** Data curation. **G. Seed:** Data curation, software, formal analysis, visualization. **I. Figueiredo:** Data curation. **M. Lambros:** Data curation. **S. Miranda:** Data curation. **A. Ferreira:** Data curation. **C. Bertan:** Data curation. **R. Riisnaes:** Data curation. **N. Porta:** Formal analysis. **W. Yuan:** Software, investigation, methodology, writing-review and editing. **S. Carreira:** Software, investigation, visualization, methodology, writing-review and editing. **J.S. de Bono:** Resources, supervision, funding acquisition.

Acknowledgments

P. Rescigno and J. Mateo were supported by a Prostate Cancer Foundation Young Investigator Award. Work in the de Bono laboratory was supported by Prostate Cancer UK and the Movember Foundation through the London Movember Centre of Excellence (CEO13_2-002), the US Department of Defense, the Prostate Cancer Foundation (20131017 and 20131017-1), Stand Up To Cancer (SU2C-AACR-DT0712), Cancer Research UK (CRM108X-A25144), and the UK Department of Health through an Experimental Cancer Medicine Centre grant (ECMC-CRM064X). A. Sharp has been supported by the Medical Research Council, the Academy of Medical Sciences, Prostate Cancer UK, and the Prostate Cancer Foundation. TOPARP-B is an investigator-initiated study supported by Cancer Research UK (CRUK/11/029, C12540 A12829, C12540/A13230, and C12540/A20447) and conducted with support from the Investigator-Sponsored Study Collaboration between AstraZeneca and the National Institute for Health Research Cancer Research Network.

The costs of publication of this article were defrayed in part by the payment of page charges. This article must therefore be hereby marked *advertisement* in accordance with 18 U.S.C. Section 1734 solely to indicate this fact.

Received June 24, 2020; revised August 17, 2020; accepted September 23, 2020; published first September 28, 2020.

References

1. Blazek D, Kohoutek J, Bartholomeeusen K, Johansen E, Hulinkova P, Luo Z, et al. The cyclin K/Cdk12 complex maintains genomic stability via regulation of expression of DNA damage response genes. Genes Dev 2011;25:2158–72.
2. Cheng SW, Kuzyk MA, Moradian A, Ichu TA, Chang VC, Tien JF, et al. Interaction of cyclin-dependent kinase 12/CrkRS with cyclin K1 is required for the phosphorylation of the C-terminal domain of RNA polymerase II. Mol Cell Biol 2012;32:4691–704.
3. Chilà R, Guffanti F, Damia G. Role and therapeutic potential of CDK12 in human cancers. Cancer Treat Rev 2016;50:83–8.
4. Juan HC, Lin Y, Chen HR, Fann MJ. Cdk12 is essential for embryonic development and the maintenance of genomic stability. Cell Death Differ 2016;23:1038–48.
5. Tien JF, Mazloomian A, Cheng SG, Hughes CS, Chow CCT, Canapi LT, et al. CDK12 regulates alternative last exon mRNA splicing and promotes breast cancer cell invasion. Nucleic Acids Res 2017;45:6698–716.
6. Ekumi KM, Paculova H, Lenasi T, Pospichalova V, Bösken CA, Rybarikova J, et al. Ovarian carcinoma CDK12 mutations misregulate expression of DNA repair genes via deficient formation and function of the Cdk12/CycK complex. Nucleic Acids Res 2015;43:2575–89.
7. Barbieri CE, Baca SC, Lawrence MS, Demichelis F, Blattner M, Theurillat JP, et al. Exome sequencing identifies recurrent SPOP, FOXA1 and MED12 mutations in prostate cancer. Nat Genet 2012;44:685–9.
8. Fraser M, Sabelnykova VY, Yamaguchi TN, Heisler LE, Livingstone J, Huang V, et al. Genomic hallmarks of localized, non-indolent prostate cancer. Nature 2017;541:359–64.
9. Cancer Genome Atlas Research Network. The molecular taxonomy of primary prostate cancer. Cell 2015;163:1011–25.
10. Linch M, Goh G, Hiley C, Shanmugabavan Y, McGranahan N, Rowan A, et al. Intratumoral evolutionary landscape of high-risk prostate cancer: the PROGENY study of genomic and immune parameters. Ann Oncol 2017;28:2472–80.
11. Abida W, Armenia J, Gopalan A, Brennan R, Walsh M, Barron D, et al. Prospective genomic profiling of prostate cancer across disease states reveals germline and somatic alterations that may affect clinical decision making. JCO Precis Oncol 2017;2017:PO.17.00029.
12. Beltran H, Prandi D, Mosquera JM, Benelli M, Puca L, Cyrta J, et al. Divergent clonal evolution of castration-resistant neuroendocrine prostate cancer. Nat Med 2016;22:298–305.
13. Grasso CS, Wu YM, Robinson DR, Cao X, Dhanasekaran SM, Khan AP, et al. The mutational landscape of lethal castration-resistant prostate cancer. Nature 2012;487:239–43.
14. Robinson D, Van Allen EM, Wu YM, Schultz N, Lonigro RJ, Mosquera JM, et al. Integrative clinical genomics of advanced prostate cancer. Cell 2015;161:1215–28.
15. Armenia J, Wankowicz SAM, Liu D, Gao J, Kundra R, Reznik E, et al. The long tail of oncogenic drivers in prostate cancer. Nat Genet 2018;50:645–51.
16. Wu YM, Cieślik M, Lonigro RJ, Vats P, Reimers MA, Cao X, et al. Inactivation of CDK12 delineates a distinct immunogenic class of advanced prostate cancer. Cell 2018;173:1770–82.
17. Rodrigues DN, Rescigno P, Liu D, Yuan W, Carreira S, Lambros MB, et al. Immunogenomic analyses associate immunological alterations with mismatch repair defects in prostate cancer. J Clin Invest 2018;128:4441–53.
18. Schreiber RD, Old LJ, Smyth MJ. Cancer immunoediting: integrating immunity's roles in cancer suppression and promotion. Science 2011;331:1565–70.
19. Fridman WH, Pagès F, Sautès-Fridman C, Galon J. The immune contexture in human tumors: impact on clinical outcome. Nat Rev Cancer 2012;12:298–306.
20. Hendry S, Salgado R, Gevaert T, Russell PA, John T, Thapa B, et al. Assessing tumor-infiltrating lymphocytes in solid tumors: a practical review for pathologists and proposal for a standardized method from the International Immunooncology Biomarkers Working Group: part 1. Assessing the host immune response, TILs in invasive breast carcinoma and ductal carcinoma *in situ*, metastatic tumor deposits and areas for further research. Adv Anat Pathol 2017;24:235–51.
21. Hendry S, Salgado R, Gevaert T, Russell PA, John T, Thapa B, et al. Assessing tumor-infiltrating lymphocytes in solid tumors: a practical review for pathologists and proposal for a standardized method from the International Immunooncology Biomarkers Working Group: part 2. TILs in melanoma, gastrointestinal tract carcinomas, non-small cell lung carcinoma and mesothelioma, endometrial and ovarian carcinomas, squamous cell carcinoma of the head and neck, genitourinary carcinomas, and primary brain tumors. Adv Anat Pathol 2017;24:311–35.
22. Barnes TA, Amir E. HYPE or HOPE: the prognostic value of infiltrating immune cells in cancer. Br J Cancer 2017;117:451–60.
23. Sundar R, Miranda S, Rodrigues DN, Chénard-Poirier M, Dolling D, Clarke M, et al. Ataxia telangiectasia mutated protein loss and benefit from oxaliplatin-based chemotherapy in colorectal cancer. Clin Colorectal Cancer 2018;17:280–4.
24. Rescigno P, Lorente D, Dolling D, Ferraldeschi R, Rodrigues DN, Riisnaes R, et al. Docetaxel treatment in PTEN- and ERG-aberrant metastatic prostate cancers. Eur Urol Oncol 2018;1:71–7.

25. Nickel JC, True LD, Krieger JN, Berger RE, Boag AH, Young ID. Consensus development of a histopathological classification system for chronic prostatic inflammation. BJU Int 2001;87:797–805.
26. Minchom A, Yuan W, Crespo M, Gurel B, Figueiredo I, Wotherspoon A, et al. Molecular and immunological features of a prolonged exceptional responder with malignant pleural mesothelioma treated initially and rechallenged with pembrolizumab. J Immunother Cancer 2020;8: e000713.
27. Sokol ES, Pavlick D, Frampton GM, Ross JS, Miller VA, Ali SM, et al. Pan-cancer analysis of CDK12 loss-of-function alterations and their association with the focal tandem-duplicator phenotype. Oncologist 2019;24:1526–33.
28. Marshall CH, Imada EL, Tang Z, Ross JS, Miller VA, Ali SM, et al. CDK12 inactivation across solid tumors: an actionable genetic subtype. Oncoscience 2019;6:312–16.
29. Reimers MA, Yip SM, Zhang L, Cieslik M, Dhawan M, Montgomery B, et al. Clinical outcomes in cyclin-dependent kinase 12 mutant advanced prostate cancer. Eur Urol 2020;77:333–41.
30. Antonarakis ES, Isaacsson Velho P, Fu W, Wang H, Agarwal N, Santos VS, et al. CDK12-altered prostate cancer: clinical features and therapeutic outcomes to standard systemic therapies, poly (ADP-ribose) polymerase inhibitors, and PD-1 inhibitors. JCO Precis Oncol 2020;4:370–81.
31. de Bono JS, Fizazi K, Saad F, Shore N, Sandhu SK, Mehra N, et al. Central prospective detection of homologous recombination repair gene mutations (HRRm) in tumor tissue from 4000 men with metastatic castration-resistant prostate cancer (mCRPC) screened for the PROfound study. Ann Oncol 2019;30: v325–v355.
32. Gagliani N, Magnani CF, Huber S, Gianolini ME, Pala M, Licona-Limon P, et al. Coexpression of CD49b and LAG-3 identifies human and mouse T regulatory type 1 cells. Nat Med 2013;19:739–46.
33. Liu Y, Carlsson R, Comabella M, Wang J, Kosicki M, Carrion B, et al. FoxA1 directs the lineage and immunosuppressive properties of a novel regulatory T cell population in EAE and MS. Nat Med 2014;20:272–82.
34. Zappasodi R, Budhu S, Hellmann MD, Postow MA, Senbabaoglu Y, Manne S, et al. Non-conventional inhibitory $CD4^{+}Foxp3^{-}PD\text{-}1^{hi}$ T cells as a biomarker of immune checkpoint blockade activity. Cancer Cell 2018;34:691.
35. Schweizer MT, Ha G, Gulati R, Brown LC, McKay RR, Dorff T, et al. CDK12-mutated prostate cancer: clinical outcomes with standard therapies and immune checkpoint blockade. JCO Precis Oncol 2020;4:382–92.